Berlin Beamforming Conference

SELECTIVE ORTHOGONAL BEAMFORMING

Robert P. Dougherty[1] and Miles H. Bridges[1]
[1]OptiNav, Inc.
1414 127th PL NE #106, 98005, Bellevue, WA, USA

ABSTRACT

In the usual setup for Beamforming there is a microphone array and a grid of potential acoustic source locations. The beamformer is expected to produce temporal spectra for the sources in the grid, or subsets of them, and images of the spatial distribution of the sources across the grid. When using a typical nonredundant array, conventional beamforming and deconvolution methods that start with conventional beamforming have very weak ability to reject interference from sources outside the grid. This can be a serious limitation for important applications including wind tunnel measurements and air taxi noise characterization. An extension of Orthogonal Beamforming (OB) rightly or wrongly to be known as Selective Orthogonal Beamforming (SOB), is proposed to address this problem. As in OB, the spectral decomposition of the array cross spectral matrix is computed and the spectral components are processed over the grid individually. For each eigenvector, the inner product of each normalized grid steering vector is computed. The grid point giving the largest inner product is the most likely location of the source responsible for the spectral component. In OB, the eigenvalue is assigned to that grid point and added to the spectrum. The modifications in SOB are that the eigenvalue is only retained if the magnitude-squared of the inner product exceeds a certain threshold and if the peak grid point is not on the border of the grid. The first criterion prevents sidelobes of strong interfering sources from being mistaken for sources of interest and the second criterion excludes low frequency interfering sources outside the grid whose main lobes are spilling over the grid. With these changes SOB is able to produce spectra for the grid, excluding interference. Another step is to reconstruct the cross spectral matrix with the interfering spectral components removed and use this as input to another beamforming/deconvolution method such as DAMAS or CLEAN-SC to produce high resolution images and integrated spectra without the effect of the interfering sources.

1 INTRODUCTION

A common use for a microphone array is to measure acoustic spectra from a region of interest (ROI) which may be a complete beamforming grid or a subset of the grid. For example, in a flight test of a reasonably quiet air vehicle, the task of a small-diameter array may be to measure the sound from the vehicle to the exclusion of inference from nearby roads, wind noise in trees, barking dogs, etc. Another example is a wind tunnel test in a facility that has not been designed to be quiet, so that interfering noise arrives from upstream and downstream of the test section. In aeroacoustic measurements such as these, the microphone array is typically a nonredundant design that operates over a wide frequency range but, as a trade-off for this ability, has a plethora of sidelobes in its point spread function (PSF) [1]. These sidelobes are known to be lower than the main peak by at least the sidelobe level (SLL), typically -7 dB. Even with full aperture sampling, i.e., an infinite number of microphones, there are sidelobes depending on the aperture shape: -20 dB for a circular disk and -13 dB for a line or rectangular array. Suppose conventional beamforming shows a peak on the beamform map when strong sources external to the beamform grid exist. This peak could represent a real source, or it could be a sidelobe from an interfering source, where the peak is lower than the full strength of the external source by at least the SLL. Another way that that interference can contaminate the conventional beamform map is that a strong, low-frequency source whose peak location is outside the beamforming grid may include some or all of the grid in the central peak of its PSF. In this case, the strength of the interference at the grid point closest to the location of the interferer will be lower than full strength by the shape of the main peak, evaluated at the offset location of the grid point. Assuming the central peak level decreases with distance from the peak location, the beamformed value of the interference will be lower at grid points other than the one closest to the interfering source.

If conventional beamforming alone is applied in a case with strong interference, then the results may be misleading. Spurious artifacts will be present in the beamforming image and the integrated spectrum will exceed the correct result for the grid or subgrid.

Numerous deconvolution techniques have been developed to improve conventional beamform maps by postprocessing [2]. In favorable situations, they can significantly improve the resolution of the images and the specificity and quantitative accuracy of component spectra. However, they generally cannot distinguish artefacts originating outside the grid from sources of interest, and may simply sharpen them.

Adaptive Beamforming [3] and Functional Beamforming [4] are able to reduce the effects of interfering noise sources by evaluating nonlinear functions of the eigenvalues of the Cross Spectral Matrix (CSM) and inner products of the eigenvectors with the array steering vectors associated with the grid points. These methods depend on tuning parameters and process one grid point at a time. They do not obviously produce quantitative spectra for ROI containing several grid points. This shortcoming may be attributable to the fact that their definitions do not acknowledge the existence of the neighboring grid points, and so do not know how to share their results. Functional Projection Beamforming [5] does account for multiple steering vectors in an ROI, but integration only works well for small ROIs and depends on tuning parameters.

2 METHOD

Suppose the array has N microphones. Withing a processing frequency band, the total power of the sound incident upon the array is taken as the sum over the microphones of the magnitude-squared of the acoustic pressure. This is the trace of CSM, $\mathrm{tr}(C)$. Dividing the sum by the number of microphones gives the array average. The spectral decomposition of C is

$$C = \sum_{i=1}^{N} \sigma_i^2 u_i u_i' \tag{1}$$

The notation σ_i^2 for the eigenvalue provides consistency with the singular value decomposition of the narrowband microphone time history matrix, if not some of the literature, such as [2].

Suppose there is a beamforming grid in 1, 2, or 3 dimensions containing a set of M_g potential source points, each having a normalized steering vector g_j that is at least approximately known. Let the unknown strength of the source at grid point j be denoted $s_j,\ j = 1, \dots, M_g$. The model for C in terms of the sources is

$$C = \sum_{j=1}^{M_g} s_j g_j g_j' + \sum_{j=1}^{M_h} n_j h_j h_j' \tag{2}$$

Here $n_j,\ j = 1, \dots, M_h$, are interfering noise source strengths from sources outside the beamforming grid with, corresponding steering vectors $h_j,\ j = 1, \dots, M_h$ points. These normalized steering vectors are not known but rather presumed to exist.

The trace of the CSM can be written

$$\mathrm{tr}(C) = \sum_{i=1}^{N} \sigma_i^2 = \sum_{j=1}^{M_g} s_j + \sum_{j=1}^{M_h} n_j \tag{3}$$

The first objective of the array measurement in the current program is to determine the total power of the sources in the beamforming grid, $\sum_{j=1}^{M} s_j$. Doing this for each frequency produces the spectrum of the sources in the grid. The determination is achieved with the aid of a key assumption: that the spectral components can be partitioned into those components associated with the grid sources and those associated with interfering sources. In other words, is it assumed that $\sum_{j=1}^{M} s_j$ is the sum of one subset of the σ_i^2 values and $\sum_{j=1}^{M_h} n_j$ is the sum the complementary set of eigenvalues.

The spectrum of the sources of interest will be ultimately be given as

$$|p|^2_{tot,interesting} = \sum_{i \in interesting} \sigma_i^2 \tag{4}$$

The spectral components are encouraged to segregate themselves in this way by choosing the grid to fill a convex region in the 1-, 2-, or 3-D beamforming space with the distance between adjacent grid point smaller than the array resolution. The g_j are somewhat parallel to their neighbors in the grid. The grid is assumed to be well separated from potential sources of interfering noise. This grid assumptions will be used in the classification algorithm to follow.

An eigenvector of C, u_i, is classified as associated with the beamforming grid, and therefore interesting, if it is more parallel to one of the grid steering vectors than to any of the interference steering vectors. This condition can be expressed as

$$\max_j \left|g_j' u_i\right|^2 > \max_j \left|h_j' u_i\right|^2 \tag{5}$$

In processing the data, the left-hand side of (5) can be evaluated directly because the eigenvectors and the grid steering vectors are known. The right-hand side has to be inferred because the h_j are not known. They describe sound sources outside the area under study. It will be seen that a necessary, but not sufficient, condition is that the LHS has to be greater than the value implied by the maximum side lobe level of the array.

This assumed partitioning of CSM into eigenvalues of interest and others is similar to the standard signal subspace picture, [6], but does not assume that the subspace of interest corresponds to the large eigenvalues. On the contrary, the interference eigenvalues may be the largest ones.

To start the classification, as in Orthogonal Beamforming (OB) [7], conventional beamforming is applied to each spectral component of C, $\sigma_i^2 u_i u_i'$. Looping over the set of grid points $j = 1, \ldots, M$, the single-component beamforming expression is:

$$b_j(u_i) = g_j'(\sigma_i^2 u_i u_i') g_j = \sigma_i^2 \left|g_j' u_i\right|^2 \tag{6}$$

The eigenvalue σ_i^2 is not actually used here but the inner product $\left|g_j' u_i\right|^2$ is evaluated to determine whether the eigenvector u_i corresponds to a source at grid location j. If there is a point source at j and nothing else is happening, then $\left|g_j' u_i\right|^2 = 1$ for $i = 1$ because the model for the CSM would be $C = s_j g_j g_j'$, matching the spectral decomposition, $s_j = \sigma_1^2$ and g_j is parallel to u_1. If there is a strong source well separated from the beamforming grid such that it corresponds to an eigencomponent of C in the interference subspace, then beamfoming this eigencompoent at its location with its steering vector, neither of which are known, would give $|h_{source}' u_i|^2 = 1$. Since the source is far from the grid, the largest value of $\left|g_j' u_i\right|^2$that is expected (in a simple case with few other sources present) is the peak sidelobe value of the array, $10^{\frac{SLL}{10}}$. For example, if the value of SSL for the array is -7 dB, then the $\left|g_j' u_i\right|^2 = \left|g_j' h_{source}\right|^2$for this interference source should not exceed 0.2.

This suggests classifying the eigenvectors using a threshold γ^2, with a typical value in the range of 0.2-0.5. For a given spectral component i, the maximum over the grid of $\left|g_j' u_i\right|^2$ is found. If this maximum is less than γ^2, then the eigenvalue σ_i^2 is classified as not of interest.

Experimentation may be necessary to choose the value of γ^2. If γ^2 is too low, then it will be too easy for eigenvectors to be assigned to the grid and the interference will not be completely removed. Using a value larger than $10^{\frac{SLL}{10}}$ can be justified on the basis that γ^2 is not too large until it results in true sources in the grid being excluded. An ideal point source in the grid would have an inner product of 1, as noted previously. Distributed sources give lower peak inner products. In the sample to follow γ^2 is set to 0.3.

If the interfering source i is not far from the beamforming grid, such that some or all of the grid is within the central peak of the PSF of the interfering source, then it should be case that the largest value $|g_j' u_i|^2$ will occur at the grid point that is closest to the interfering source. This depends on an assumption that the PSF inside the central peak decreases monotonically away from the source location. With a reasonable assumption about the shape of the grid, such as convexity, the largest value of $|g_j' u_i|^2$ over j will occur on the boundary of the grid if the source is outside the grid but the grid is overlapping the central peak. (In the intermediate case where the central peak touches the grid but the PSF maximum is interior to the grid, then the γ^2 classification will apply and the eigencomponent should be appropriately rejected.) This suggests a second criterion for classifying eigencomponents as not of interest: if the peak of $|g_j' u_i|^2$ is on the boundary of the grid.

For each eigencomponent i of C, if it passes both tests: $\max_j |g_j' u_i|^2 \geq \gamma^2$ and $j_{max} = \mathrm{argmax}\left(|g_j' u_i|^2\right) \notin \partial\mathrm{grid}$, then σ_i^2 is added into the spectrum of the array output for the method.

Note that the boundary classification is very sharp, even at very low frequency. The source peak is in the interior of the grid or it is not.

It is appropriate to revisit the connection between the eigenvector classification algorithm and the logic of Eqs. (2) and (5). The assumption driving the classification is that the beamfoming-grid and interference subspaces are distinct and an eigenvector of C belongs to one or the other. The classification algorithm is used to identify the situation for each eigenvector. An eigenvector that belongs to the interference subspace is considered to correspond to a steering vector, h in Eq. (2) that is parallel to the eigenvector. In this case, the RHS of Eq. (5) is unity and the condition is clearly false: the eigenvector is not associated with the beamforming grid. The classification method is intended to detect this situation by its fallout using the beamforming grid: only a small peak can be found in the interior of the grid, consistent with a sidelobe, or the maximum value of the inner product is on the boundary, consistent with peak spillover. If an eigenvector cannot be dismissed as interference then it is considered to be associated with the grid. In this case, the LHS of Eq. (5) is at least the threshold value. The value of the right hand side is difficult to know because, while the eigenvector is known, the interference steering vectors are not.

After isolating the eigencomponents C that correspond to sources in the grid, it is possible to reconstruct an edited version of C:

$$C_{interesting} = \sum_{i \in interesting} \sigma_i^2 u_i u_i' \tag{7}$$

This can be used in a beamforming/deconvolution method such as DAMAS or CLEAN-SC, which should then be able to make effective source images and collect integrated spectra over small ROIs for components in the grid.

3 EXAMPLE

The string trimmer data from [5] is reused here. As show in Fig. 1, a 40-channel microphone array sampled at 50 kHz with an aperture of about 0.3 m is positioned 2 m from a suitably oriented string trimmer. The string produces distributed, broadband, self noise as it rotates. It is louder in the portion of the disk where the string is approaching the array due to Doppler amplification. The motor of the string trimmer contributes a few tones. Foam rubber on part of the floor and several other surfaces reduces reflections for propagation from the string trimmer to the array. Interfering noise is produced by a loudspeaker as shown. The positioning of the loudspeaker above and somewhat behind the array was intended to create a partially diffuse sound field due to reverberation in the facility and diffraction around the array. The level of the pink noise supplied to the loudspeaker was gradually increased during the run over about 45 s. Two 1-second segments were selected from the recording: the first has low interference, supplied mostly by the industrial setting of OptiNav, Inc. The second segment is near the end of the recording and has much more noise than signal from the sting trimmer over most of the frequency range. Results from processing this segment are referred to as the case with interference.

Narrowband SOB integrals with and without interference are compared in Fig. 2. In this and all the plots to follow, γ^2 is set to 0.3. The ROI is the entire image shown in Figs. 3-10. Reference curves of the array median SPL values with and without interference are also shown. The SNR, the difference between the two median curves, varies from -18 dB at 2100 Hz to 0 at 20 kHz. The difference between the array median with no interference and the integral with no interference, about 2 dB, can be attributed mostly to imperfect absorption of reflected paths by the foam rubber treatment on the floor and the top and sides of the test arena. Sound in these paths contributes to the array median but is excluded from the SOB integration ROI. The curve for the SOB integral with interference is generally within 2 dB of the corresponding curve to no interference. It was necessary to tune the value of γ^2 to achieve this result in this challenging case. The value of 0.3 has also been found to be effective in less-difficult situations with this array. Is not known whether there are other problems for this array that are feasible for the method but would require a different value of γ^2.

Use of SOB as a prefiltering step for beamforming methods is explored in Figs. 4-10. Each figure shows four 1/12 OB beamforming images. The image at the upper left represents beamforming or beamforming followed by deconvolution for the case of data with no interference and no SOB prefiltering. The effect of the interfering noise without SOB prefiltering is shown at the upper right. In each case, the interference significantly distorts the results. As a check, the effect of processing the interference-free data with SOB prefiltering is shown in the lower left. In most cases, the effect is minor. Finally, data with interference is prefiltered with the SOB intended to remove the is shown at the lower right. Success is indicated by the agreement between the lower right image with the upper left. Figures 4&5 give this presentation at for conventional beamforming at 4 kHz and 8459 Hz, respectively. Figures 6&7 and 7&8 repeat these frequencies for DAMAS and CLEAN-SC, respectively. The selected frequency bands include small motor tones as seen Fig 2 and 4-10.

The conventional beamforming results in Figs. 4&5 demonstrate the utility of SOB prefiltering. The image from the contaminated data in the upper right of Fig. 3 for 4 KHz shows almost no relationship to the uncontaminated case in the upper left. The filtered result at the lower right is similar to the uncontaminated case. At 8459 Hz, the results are similar, except the motor tone is missing from this plot. It also missing for the deconvolutions plots in Figs. 7&9, suggesting that the eigenvalue processing has incorrectly removed the motor noise for this case.

Figures 6&7 show that DAMAS struggles to resolve the shape of the string trimmer noise distribution at that 4 kHz but resolves the motor noise clearly. As in the conventional case, the plot with interference and no filtering shows contamination. At 8459 Hz, DAMAS can resolve a ring source for the string trimmer noise, but not with interference and no filtering. The ring is less clear for the case of filtering with interference and the motor noise is missing again.

CLEAN-SC, Figs. 8&9, does not resolve the ring source. The upper right plot in Fig. 9 for 8459 Hz for interference and no filtering has an arrangement of spots that somewhat resembles the ring, but is it probably just a coincidental arrangement sidelobes from the interference. With some imagination, the 70 dB sidelobe spot in the upper right of Fig. 5 that leads to the spot just below the hub in Fig. 9 can be identified.

Figure 10 shows that Robust Functional Beamforming [8] (RFB) can also remove the effect of interference from the beamform maps. The motor noise at 8459 Hz is not removed. Unlike SOB, RFB is not ideally suited to integration.

One-twelfth octave band integration spectra for the data with interference are shown in Fig. 10. The sequence for computing these spectra was to first apply SOB prefiltering using the entire image as the ROI for some of the curves. In other cases, shown as dashed lines, prefiltering was not used. A beamforming/integration method was applied to the filtered and unfiltered data, giving results as shown in Figs. 4-9. The results were integrated over a rectangular ROI that included the string disk and the motor, but was smaller than the complete image, as shown in Fig. 3. In the case of conventional beamforming, the integral was normalized by the integral of the theoretical point spread function. No points were excluded from any of integrals by a threshold. Figure 11 gives curves for conventional beamforming, DAMAS, and CLEAN-SC. Other curves are shown for reference: the array median spectrum (the highest curve in the plot), the SOB eigenvalue integral (generally the lowest curve), and an estimate of the correct spectrum. Unlike the other curves, the correct estimate was derived from the data without interference. It was taken to be the array median spectrum with no interference, reduced by 2 dB to compensate for reflection from foam rubber surfaces as discussed previously.

All three integrals in Fig. 11 are well above the correct curve, by more than 10 dB at some frequencies. This is a result of integrating sidelobes of the interfering noise. Among the curves using SOB, the highest, and least correct, one is conventional beamforming, FDBF. It is 2-5 dB above the correct curve. The next lower curve is the SOB eigenvalue integral. It is about 2 dB above the correct curve. The excess can be interpreted as reflections of the true source and interference noise from the foam surfaces in between the SOB ROI and the, smaller, source ROI in Fig. 3. The integrals of the deconvolution results for the SOB-prefiltered data are close to the correct curve with CLEAN-SC closer than DAMAS at most frequencies.

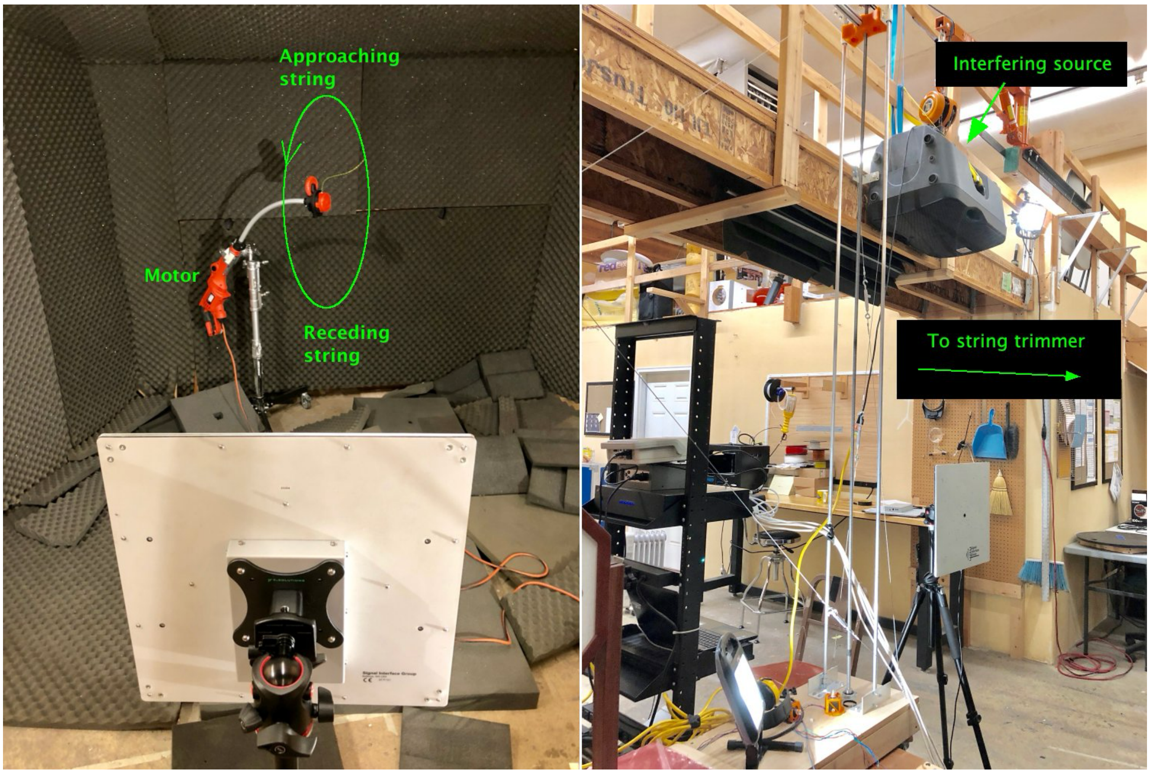

Fig.1. String trimmer test setup from [5]. Left: back of microphone array and string trimmer. Right: interfering loudspeaker located above the microphone array.

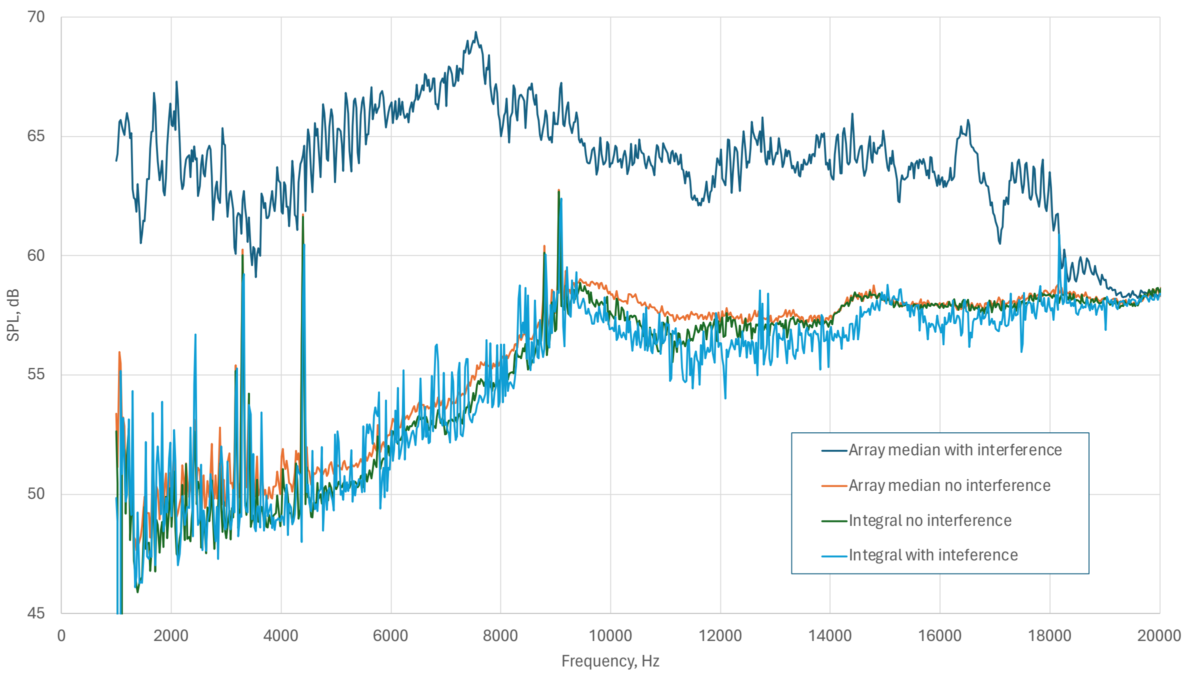

Fig.2. String trimmer spectra for microphone median and Selective Orthogonal Beamforming with and without interference.

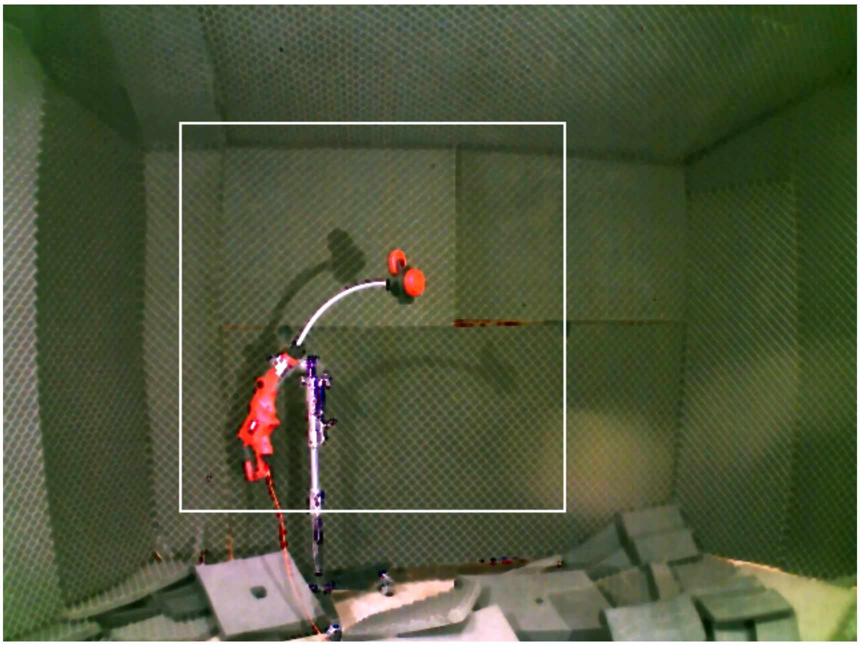

Fig.3. Regions of Interest for Selective Orthognal Beamforming: the entire image, and for integration results from conventional beamforming and deconvolution: the white box.

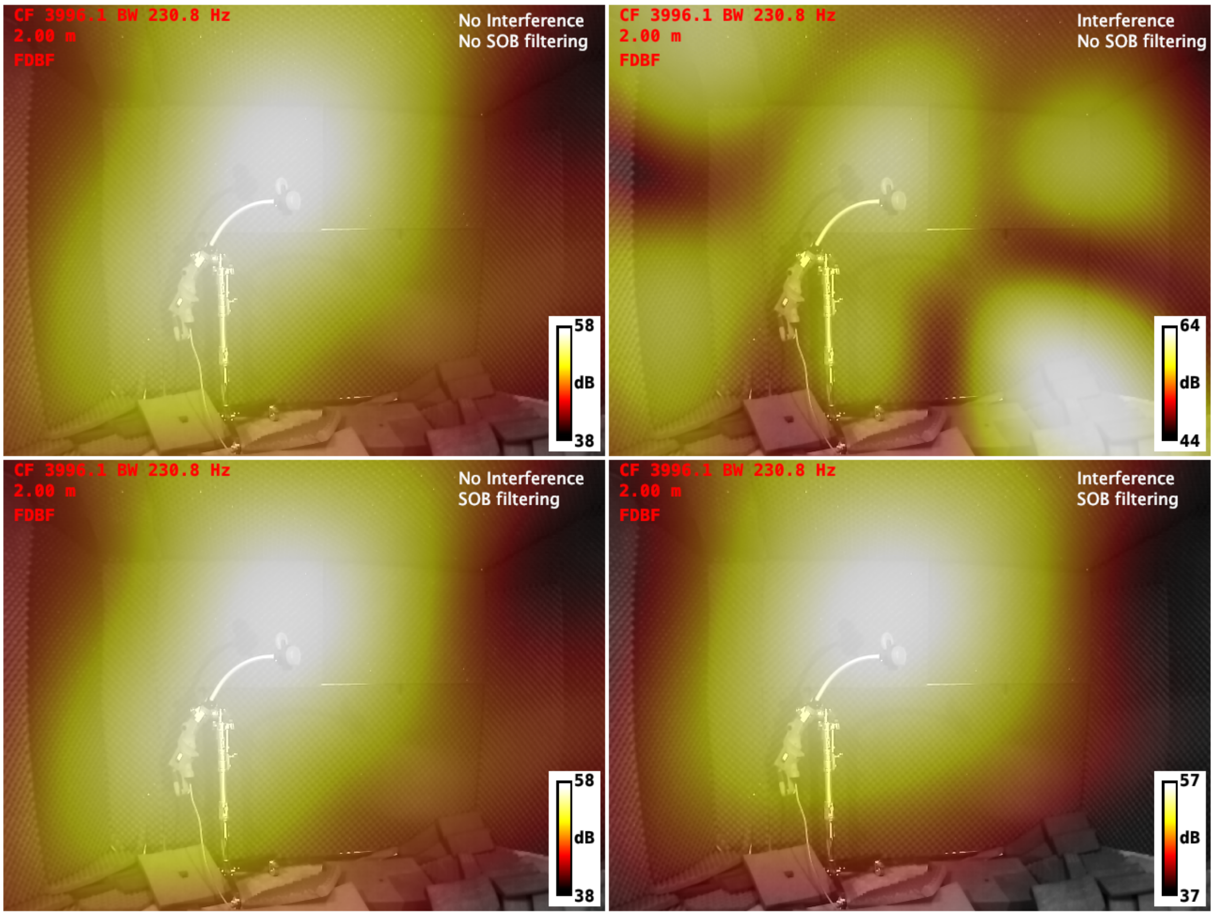

Fig.4. Conventional beamforming applied to string trimmer data with and without interference and with and without SOB prefiltering as indicated at the upper right 4000 Hz 1/12 OB.

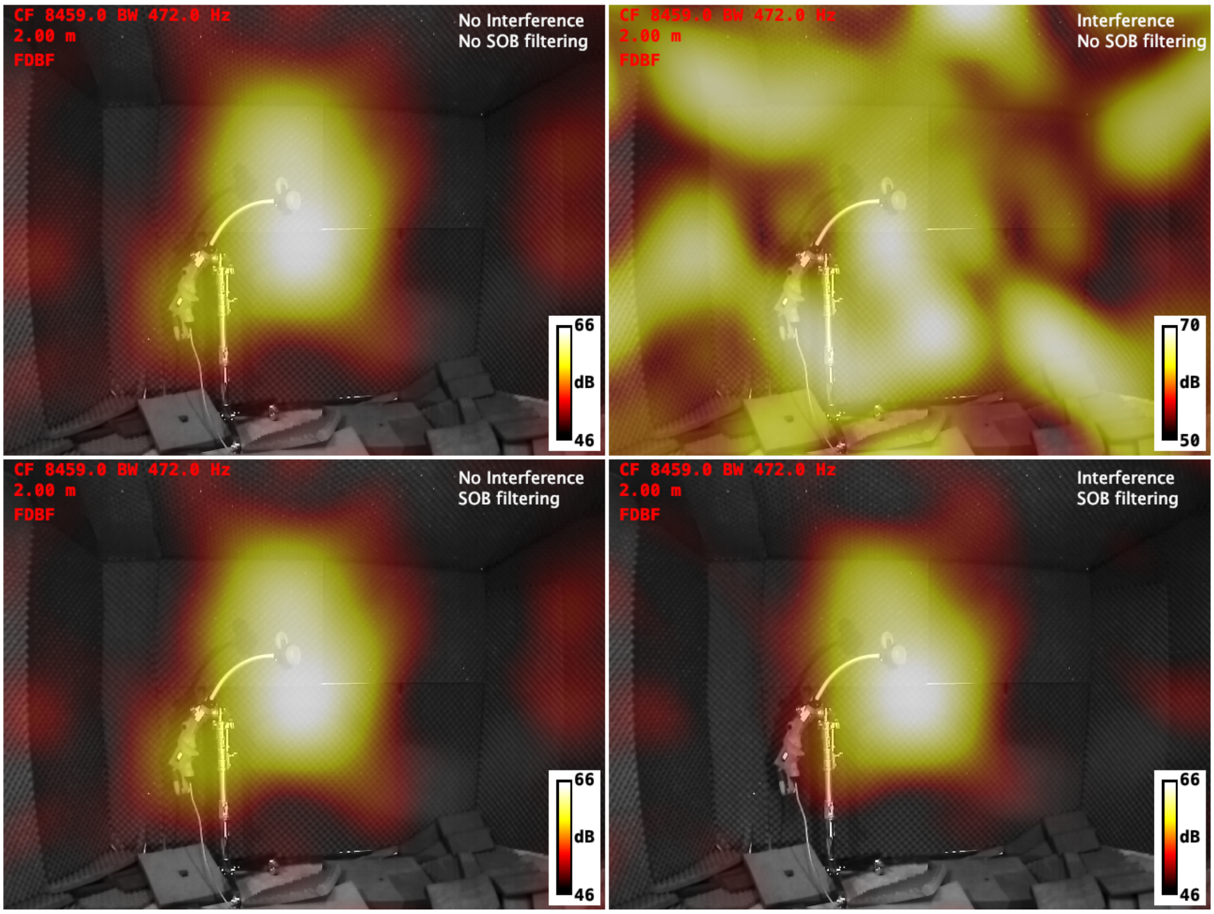

Fig.5. Conventional beamforming applied to string trimmer data with and without interference and with and without SOB prefiltering as indicated at the upper right 8459 Hz 1/12 OB.

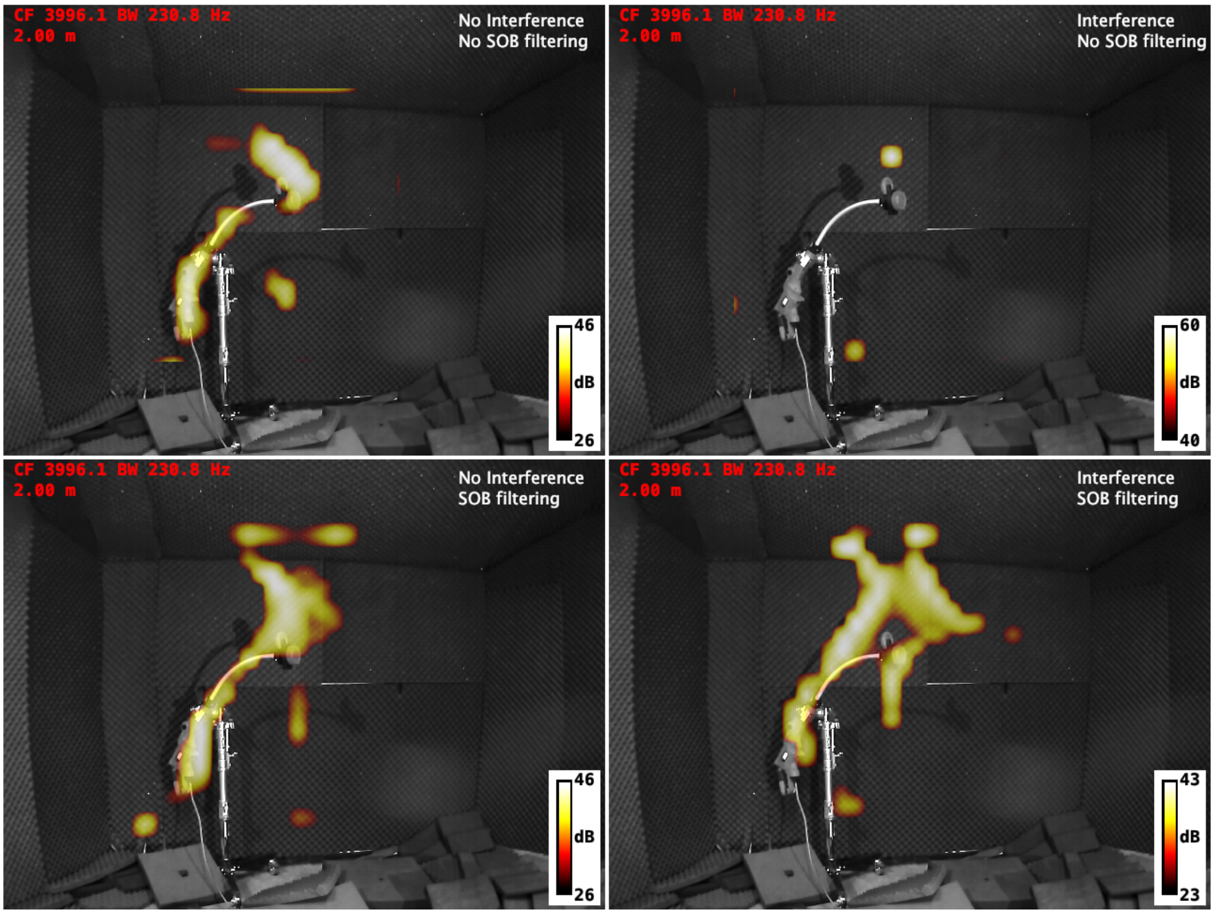

Fig.6. DAMAS applied to string trimmer data with and without interference and with and without SOB prefiltering as indicated at the upper right 4000 Hz 1/12 OB.

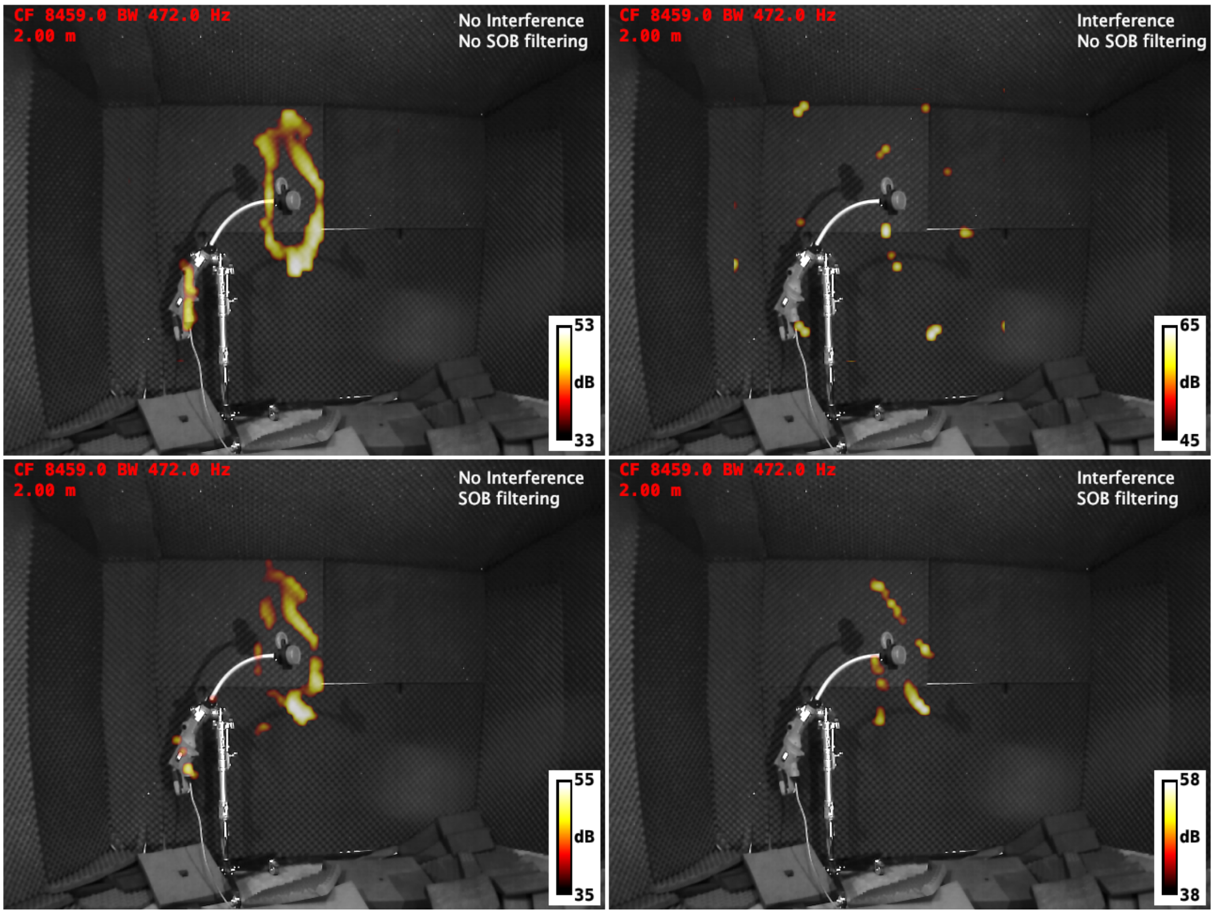

Fig.7. DAMAS applied to string trimmer data with and without interference and with and without SOB prefiltering as indicated at the upper right 8459 Hz 1/12 OB.

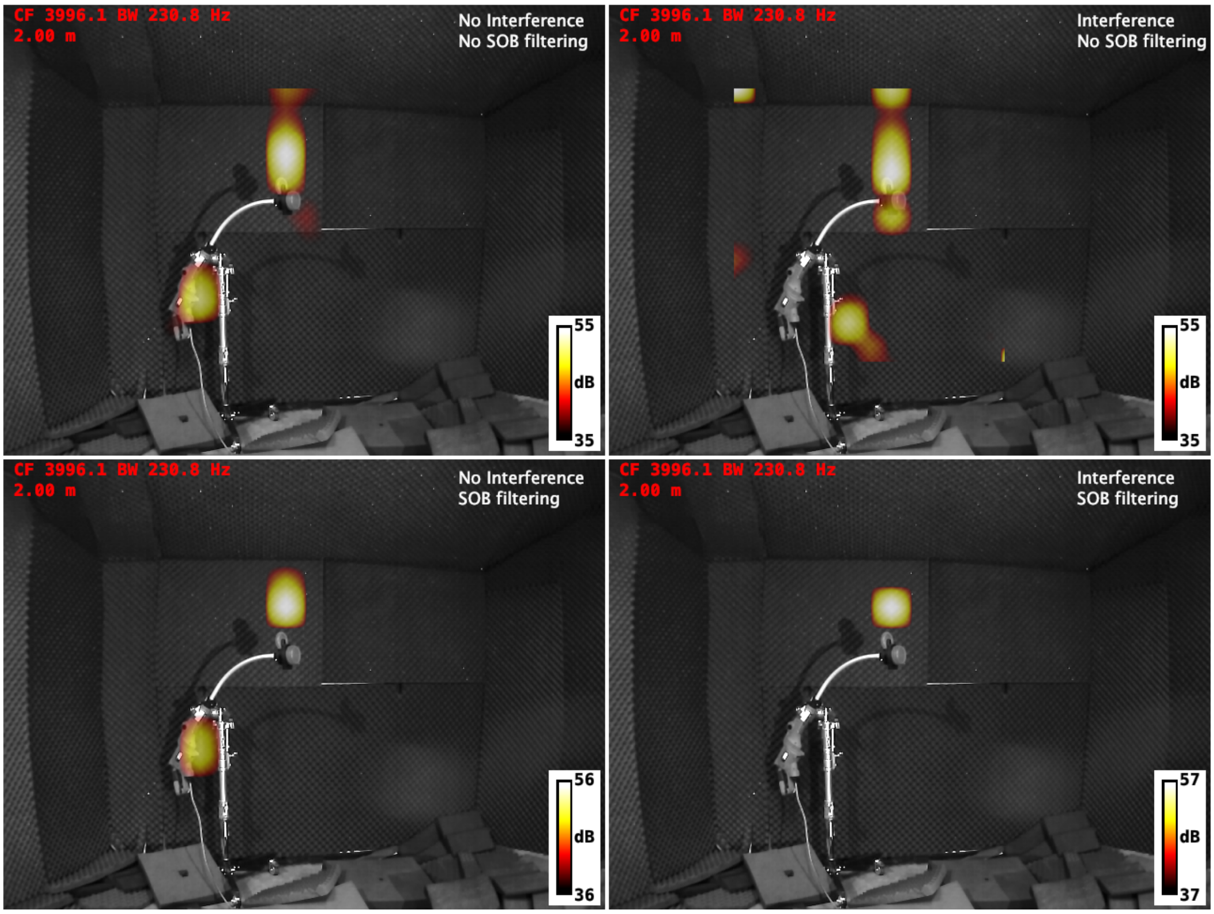

Fig. 8. CLEAN-SC applied to string trimmer data with and without interference and with and without SOB prefiltering as indicated at the upper right 4000 Hz 1/12 OB.

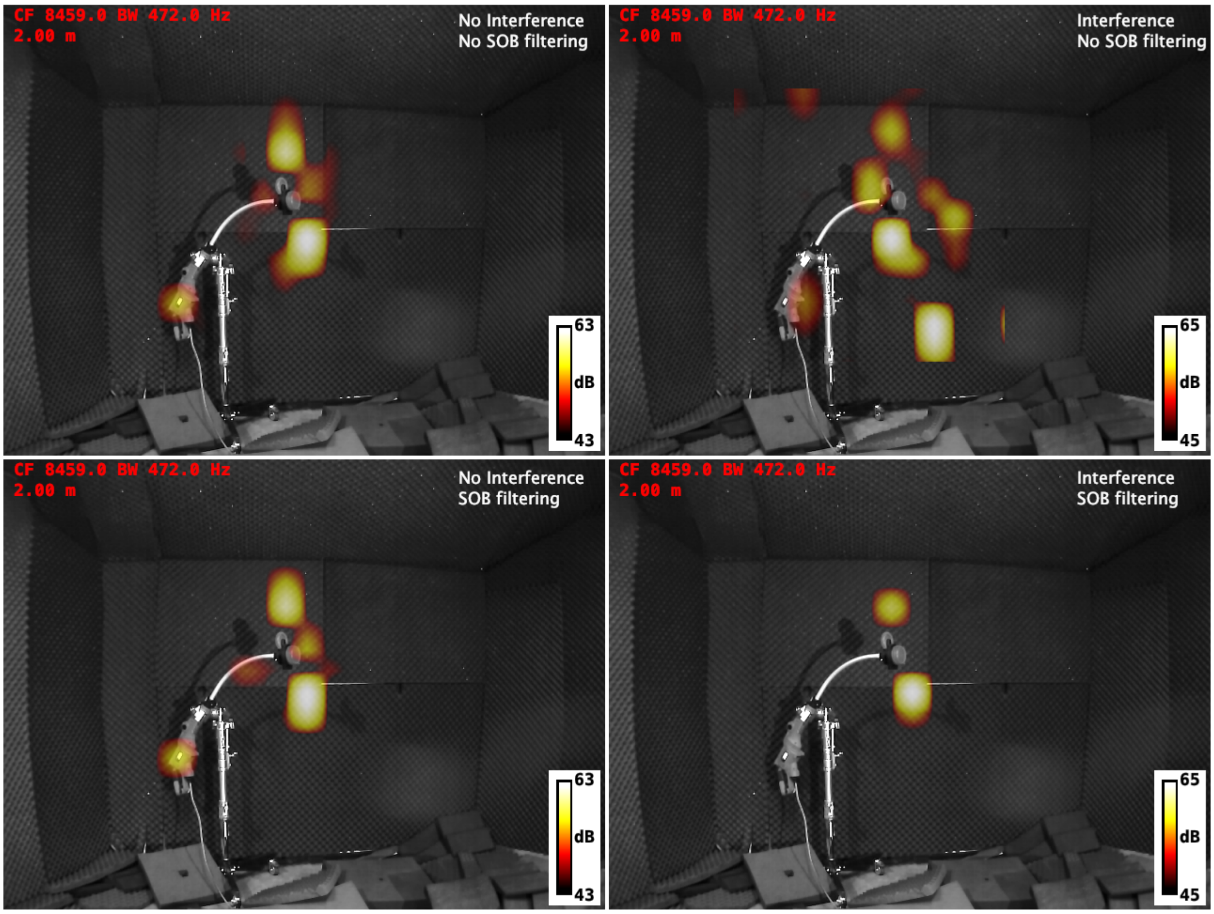

Fig. 9. CLEAN-SC applied to string trimmer data with and without interference and with and without SOB prefiltering as indicated at the upper right 8459 Hz 1/12 OB.

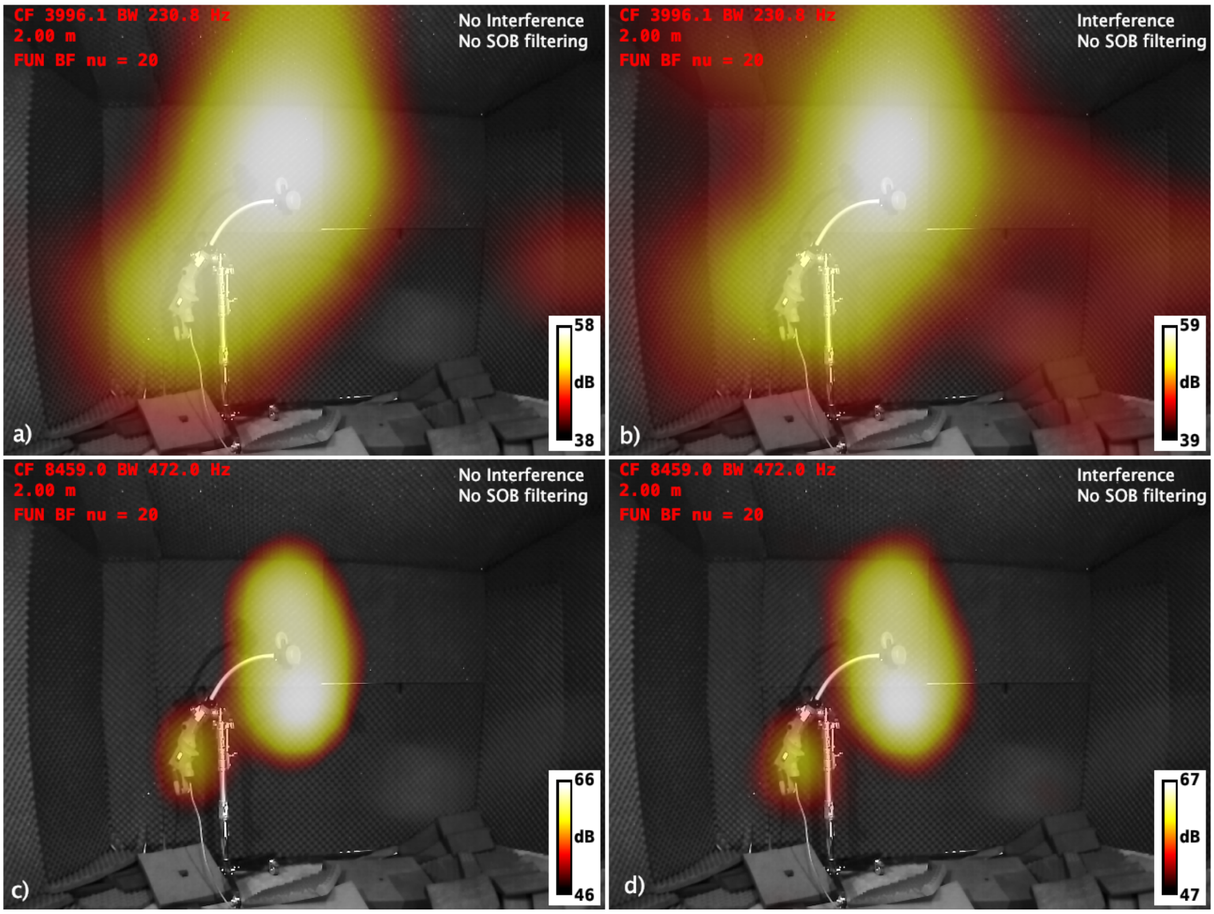

Fig. 10. Robust Functional Beamforming ($\nu = 20, t = 0.1, 1/12\ OB$) applied to string trimmer data without SOB filtering. a) 4000 Hz & no interference, b) 4000 Hz with interference, c) 8459 Hz & no interference, d) 8459 Hz with interference. Compare with the top rows of Figs. 3 & 4.

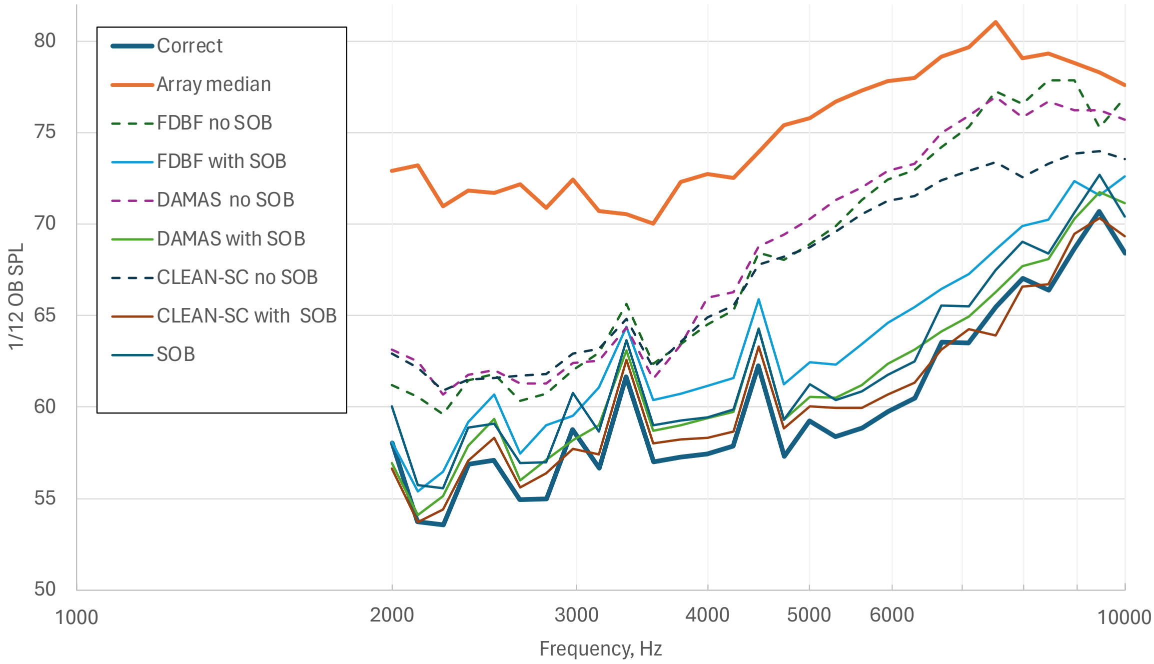

Fig.11. Results of integrating the data with interference over an ROI containing the string trimmer string and motor (the white box in Fig. 3) using various methods with and without SOB prefiltering. The SOB ROI was the complete image in Figs. 3. Also shown are the array median spectrum and an estimate of the correct spectrum for the source ROI that was computed by subtracting 2 dB from the array median without interference.

4 CONCLUSIONS

Selective Orthogonal Beamforming offers a simple way to remove interfering noise from microphone array data. The results can be used directly as cleaned-up array-average spectra and can also be applied to update the CSM to improve subsequent beamforming. For a simple case such as measuring the noise from an aircraft where the interfering sources are well separated from the intended sources, the SOB eigenvalue integral can be applied by itself. If the part of the interference, which may be other sources on the vehicle outside the intended ROI are too close for the eigenvalue method to be effective, then it may be effective to apply SOB filtering followed by conventional beamforming and then possibly deconvolution and integration. This process was tested in an example using DAMAS and CLEAN-SC. Best results for images were obtained using DAMAS and for an integral using CLEAN-SC. It was demonstrated that DAMAS and CLEAN-SC can fail in the presence of off-grid interference and the SOB integral and SOB prefiltering can recover from the interference. Separately, it was also shown that Robust Functional Beamforming can overcome strong interference for images.

5 ACKNOWLEDGEMENT

Selective Orthogonal Beamforming was developed under the Navy SBIR project “Predictions of the Acoustic Nearfield on a Carrier Deck”, contract N68335-19-C-0528.

REFERENCES

[1] Underbrink JR and RP Dougherty, Array design for non-intrusive measurement of noise sources. Proc. Noise-Con 96. 1996.

[2] Merino-Martınez, R. et al. A review of acoustic imaging methods using phased microphone arrays: Part of the “Aircraft Noise Generation and Assessment” Special Issue. CEAS Aeronautical Journal 10, 197–230 (2019).

[3] Cox, H., Zeskind, R. & Owen, M. Robust adaptive beamforming. IEEE Transactions on Acoustics, Speech, and Signal Processing 35, 1365–1376 (1987).

[4] Dougherty, R.P., “Functional Beamforming”, Berlin Beamforming Conference, BeBeC 2014-1, 2014.

[5] Dougherty, R. P. Determining spectra of aeroacoustic sources from microphone array data in 25th AIAA/CEAS aeroacoustics conference (2019), 274.

[6] Schmidt, R. Multiple emitter location and signal parameter estimation. IEEE Transactions on Antennas and Propagation 34, 276–280 (1986).

[7] Sarradj, E. Quantitative source spectra from acoustic array measurements in 2nd Berlin Beamforming Conference (2008).

[8] Dougherty, R.P. Robust Functional Beamforming in 9th Berlin Beamforming Conference (2022).